Available online at www.sciencedirect.com
SCIENCE DIRECT
Polymer 46 (2005) 8141–8150
polymer
www.elsevier.com/locate/polymer

Wide angle X-ray diffraction investigation of crystal orientation in miscible blend of poly(ε-caprolactone)/poly(vinyl chloride) crystallized under strain

Yubao Zhang[a], Véronique Leblanc-Boily[b], Yue Zhao[c,*], Robert E. Prud'homme[a,*]

[a]*Département de chimie, Université de Montréal, C.P. 6128, Succursale Centre-ville, Montréal, Que., Canada H3C 3J7*
[b]*Département de Chimie, Université de Laval, Sainte-Foy, Que., Canada GIK 7P4*
[c]*Département de Chimie, Université de Sherbrooke, Sherbrooke, Que., Canada J1K 2R1*

Received 24 February 2005; received in revised form 22 June 2005; accepted 29 June 2005

Abstract

The orientation of poly(ε-caprolactone) crystals in miscible poly(ε-caprolactone)/poly(vinyl chloride) (PCL/PVC) blends, melt crystallized under strain, has been studied by wide angle X-ray diffraction (WAXD). At low draw ratios or low PVC contents, all the observable (*hk*0) crystal reflections orient towards the meridional direction in WAXD patterns, indicating the presence of ring-fibre orientation. With the increase of draw ratio or PVC content, additional crystal orientation with the crystal *a*-axis parallel to the stretching direction is found to superimpose on the WAXD pattern of ring-fibre orientation. Both the ring-fibre orientation, which dominates the WAXD pattern, and the *a*-axis orientation are characterized by the perpendicular orientation of the crystal *c*-axis to the stretching direction. The unusual PCL orientation is a consequence of the combined effects of both the stretching and the presence of PVC in the PCL/PVC blends.

Keywords: PCL/PVC blends; Crystal orientation; X-ray diffraction

1. Introduction

Several industrial techniques for polymer processing, such as fibre spinning and film extrusion, involve the crystallization from a pre-oriented melt [1–3]. It is known that the orientation of polymer chains in the melt speeds up the rate of crystallization, and results in morphologies substantially different from those of the corresponding quiescent melt, for example in shish-kebab morphologies [1–7]. Generally, the orientation of polymer chains in a melt is expected to induce the formation of primary nuclei, and the polymer chain axis (or the crystal *c*-axis for most systems) to orient parallel to the direction of deformation by epitaxial growth of polymer crystals from the oriented nuclei.

In a recent publication, the orientation of poly(ε-caprolactone) in a model miscible blend of poly(ε-caprolactone)/poly(vinyl chloride) (PCL/PVC), melt crystallized under strain, has been investigated [8]. In contrast with the conventional crystal orientation in uniaxially stretched polymers, where the polymer chain axis is usually parallel to the stretching direction, crystal orientation with chain axis perpendicular to the stretching direction has been observed. The extent of orientation and its variation with draw ratio and composition have been characterized by Herman's orientation function ($\langle P_2 \rangle$) through infrared (IR) dichroism measurements. The $\langle P_2 \rangle$ of the PCL crystal phase was in many cases close to -0.5, indicating the perpendicular orientation of the polymer chain axis with respect to the stretching direction. The amorphous PCL chains, however, were found only slightly oriented to the stretching direction. While IR dichroism analysis has the advantage of measuring the segmental orientation of PCL chains in both crystal and amorphous phases, it provides only the average degree of

* Corresponding authors. Address: Department of Chemistry, Université de Montréal, 2900, Boul. Edouard-Montpetit, C.P. 6128, Downtown Area, Montreal, Que., Canada H3C 3J7. Tel.: +1 514 343 6730; fax: +1 514 343 7586.
E-mail address: re.prudhomme@umontreal.ca (R.E. Prud'homme).

0032-3861/$ - see front matter © 2005 Elsevier Ltd. All rights reserved.
doi:10.1016/j.polymer.2005.06.114

orientation of polymer chains in crystals. Information about the orientation of individual crystal axes as well as their distributions are missing from the IR dichroism analysis.

In the present work, we employed wide angle X-ray diffraction (WAXD) to determine the crystal orientation of PCL/PVC blend films melt crystallized under strain. Two kinds of crystal orientations, i.e. ring-fibre orientation and *a*-axis orientation, were found to coexist in the PCL/PVC blends. Both of them are characterized by the perpendicular orientation of the crystal *c*-axis to the stretching direction, with the ring-fibre orientation dominating the WAXD patterns. Orientation information of individual crystal axes has been obtained from the analysis of two-dimensional WAXD patterns. Furthermore, the increase of draw ratio and PVC content in PCL/PVC blends leads to the preferential orientation of the crystal *a*-axis to the stretching direction.

2. Experimental section

2.1. Samples

The polymer samples used to prepare PCL/PVC blends are commercially available PCL (Aldrich, $M_w = 18,000$ g/mol) and PVC (Shawinigan Chemicals, $M_w = 160,000$ g/mol). Thin films of PCL/PVC blends for stretching and X-ray analysis were prepared by casting 5% THF solutions onto the surface of a petri dish and then dried under vacuum at 40 °C for 1 week to eliminate the residual solvent. Three PCL/PVC blends containing 59.3, 71.1 and 80.3 wt% of PCL were used in this study and are identified as PCL/PVC-60/40, PCL/PVC-70/30 and PCL/PVC-80/20, respectively. The film thickness is around 200 μm, and films with size $\sim 5 \times 50$ mm^2 were used for stretching experiments. In a typical experiment, a solution cast film was heated to 90 °C for 30 min in order to remove its thermal history and, then, rapidly cooled down to room temperature. The blend films were stretched at a strain rate of 20 mm/min immediately after cooling. The stretched samples were then crystallized at room temperature under strain. Usually, stretched samples were kept on the stretcher for at least 4 h for the completion of crystallization, and X-ray measurements were performed within 1 week after sample preparation.

2.2. X-ray diffraction measurements

WAXD measurements were carried out with a Bruker diffractometer (Siemens Kristalloflex 780 generator), operated at 40 kV and 40 mA, using sealed tube Cu Kα (1.542 Å) radiation collimated by a graphite monochromator and 0.5 mm pinhole; the diffraction pattern was captured by an AXS two-dimensional wire-grid detector (HI-STAR). Fig. 1 shows the stretching geometry of PCL/PVC blend samples, where DD is the deformation (stretching) direction, ND is the normal direction, and TD is the transverse direction. For WAXD measurements, the incident X-ray beam is in the ND direction, unless otherwise indicated.

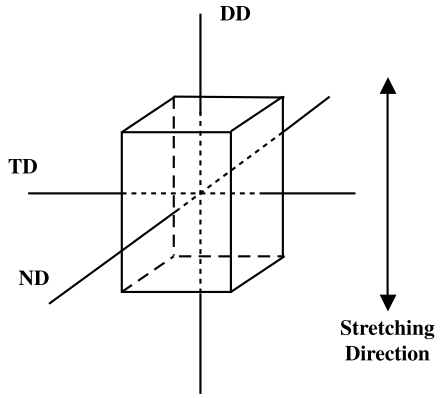

Fig. 1. Stretching geometry of PCL/PVC samples, where DD is the deformation (stretching) direction, ND is the normal direction, and TD the transverse direction.

PCL was known to have a polyethylene-like crystal structure with the orthorhombic unit cell parameters $a = 0.748$ nm, $b = 0.498$ nm and $c = 1.729$ nm [9]. In a typical powder X-ray diffraction pattern of PCL/PVC blends, two strong reflection rings at Bragg angles $2\theta = 21.4°$ and $2\theta = 23.7°$ are clearly observed. These reflections have been attributed to the (110) and (200) reflections, respectively [10], although the (200) reflection is actually the overlap of the strong (200) reflection and the much weaker reflections of (201), (112), (013) and (104) [9].

The orientation of PCL orthorhombic crystals was investigated using mainly the two strongest reflections at Bragg angles $2\theta = 21.4°$ and $2\theta = 23.7°$. The azimuthal distribution, i.e. the variation of diffracted intensity $I(\chi)$ with azimuthal angle χ was obtained by integration over $2\theta \pm \Delta\theta$ degree around the peak position. In order to determine a proper $\Delta\theta$, a series of azimuthal scans of various $\Delta\theta$ were made; Herman's orientation function $\langle P_2 \rangle$ were calculated and found to slightly decrease with decreasing $\Delta\theta$ for $\Delta\theta < 1.0°$, and to level off after $\Delta\theta \sim 0.3°$. Therefore, $\Delta\theta = 0.2°$ was used for the calculation of azimuthal scans. The corrected intensity $I^*(\chi)$ was obtained by subtracting the background values, estimated from the WAXD profile of $I \sim 2\theta$ by curve fitting, at $2\theta = 21.4$ and 23.7°, respectively. Here we assume that the amorphous orientation, if any, has little influence on the azimuthal background profile.

Before calculating the orientation function, the azimuthal angles χ on the two-dimensional detector were corrected to φ, the angle between the DD direction and the normal of individual crystal planes, using the following equation [11]:

$$\cos\varphi = \cos\theta \cos\chi \tag{1}$$

The orientation distribution function, $N(\varphi)$, of a given reflection may be reconstructed by [12]:

$$N(\varphi) = \sum_{n=0}^{\infty}(n + 1/2)\langle P_n\rangle P_n(\cos\varphi) \quad (2)$$

where the $\langle P_n\rangle$ coefficients are calculated according to the equation [13]:

$$\langle P_n\rangle = \frac{\int_0^{90} I^*(\varphi)P_n(\cos\varphi)\sin\varphi\,\mathrm{d}\varphi}{\int_0^{90} I^*(\varphi)\sin\varphi\,\mathrm{d}\varphi} \quad (3)$$

$\langle P_n\rangle$ values calculated from the (h00), (0k0) and (00l) planes characterize the degree of orientation of crystal a-, b- and c-axes, respectively, and $\langle P_n\rangle_{001}$ provides a measure of molecular chain orientation since the crystal c-axis is parallel to the chains. For PCL, the intensity of the (00l) reflection is weak, the c-axis orientation $\langle P_n\rangle_c$ can be calculated from the (110) reflection by [14]:

$$\langle P_n\rangle_c = \frac{\langle P_n\rangle_{110}}{P_n(\cos\phi_{110})} \quad (4)$$

where ϕ_{110} is the angle between the normal to the (110) plane and the c-axis. This equation holds if the orientation distribution possesses cylindrical symmetry around the deformation direction [13,14].

In this study, we focused on the second moment of the orientation function, or Herman's orientation function, for the a-, b-, and c-axes, i.e. $\langle P_2\rangle_a$, $\langle P_2\rangle_b$ and $\langle P_2\rangle_c$. Among these, $\langle P_2\rangle_a$ was obtained directly from Eq. (3), while $\langle P_2\rangle_c$ was calculated from $\langle P_2\rangle_{110}$ by using Eq. (4). The $\langle P_2\rangle_b$ was then estimated from:

$$\langle P_2\rangle_a + \langle P_2\rangle_b + \langle P_2\rangle_c = 0 \quad (5)$$

In the calculation of $\langle P_2\rangle_a$, since the (200) reflection is interfered by contributions from (013), (112) and (104) reflections, the azimuthal profile at $2\theta = 23.7 \pm 0.2^\circ$ was fitted by Pearson VII functions. The decomposed azimuthal profile of the (200) reflection was employed to calculate $\langle P_2\rangle_a$ using Eq. (3), in which the contribution of the azimuthal peak at $\chi \sim 65^\circ$ was excluded.

3. Results

3.1. The development of PCL crystallization under strain

Fig. 2 shows a set of typical WAXD patterns recorded at various times of a PCL/PVC-80/20 blend film stretched to $\lambda = 3.6$ and crystallized at room temperature ($\sim$22°) under strain. The initial pattern [$t = 50$ s, Fig. 2(a)], shows a typical amorphous halo, indicating that there is no residual crystal in the stretched polymer melt. After an induction period of about 250 s, sharp (110) and (200) crystal reflections start to emerge [Fig. 2(b)]. The existence of orientation is immediately apparent from the arced nature of the reflections. The characteristics of the WAXD patterns do not change during crystallization [Fig. 2(b)–(f)], implying that the subsequent crystallization process contributes merely to increase the PCL crystallinity. The corresponding azimuthally averaged WAXD profiles are shown in Fig. 3. The intensity of crystal reflections increases with the crystallization time. After about $\sim$1150 s, no significant intensity change is observed for all the crystal reflections in the diffraction pattern, indicative of the completion of crystallization. These observations of PCL crystal development in stretched PCL/PVC-80/20 blend film are in agreement with previous IR dichroism and DSC results [8].

3.2. Characteristic features of the orientation of PCL/PVC blends melt crystallized under strain

Figs. 4(a)–(c) show typical WAXD patterns along ND, TD and DD directions, respectively, for a PCL/PVC-80/20 blend crystallized from a pre-oriented melt (hereafter called melt-drawn sample); the WAXD pattern (ND direction) of a PCL/PVC blend crystallized from quiescent melt, and then stretched at room temperature ($\sim$22 °C) to a similar draw ratio (hereafter called cold-drawn sample), is also shown for comparison [Fig. 4(d)]. The WAXD patterns along ND and TD directions are essentially identical and exhibit clear orientation for both (110) and (200) reflections. The WAXD pattern along DD direction, however, shows two strong (110) and (200) reflections with no orientation. These patterns indicate that PCL crystals are randomly distributed in the ND-TD plane with the symmetric axis parallel to the DD direction. This behavior is one of the characteristics of an uniaxially stretched polymer sample and was observed in PCL/PVC blends crystallized from pre-oriented melts of various draw ratios and compositions. Therefore, only the diffraction patterns along the ND direction are displayed and analyzed in the following paragraph.

A comparison between the melt-drawn and the cold-drawn samples reveals that, although both samples show the presence of orientation, the crystal c-axis in the cold-drawn sample is oriented along the stretching direction as is evidenced by the higher intensity of both (110) and (200) reflections on the equator. In contrast, the melt-drawn sample shows a different orientation, since both the (110) and (200) reflections are concentrated on the meridian instead of the equator. PCL is known to have a polyethylene-like crystal structure with orthorhombic unit cell. Both (110) and (200) reflections are perpendicular to the crystal c-axis [9]. Therefore, the preferential distribution of (110) and (200) reflections along the meridian indicates perpendicular orientation of the crystal c-axis to the stretching direction. These WAXD measurements thus confirm the previous conclusion from IR dichroism analysis, i.e. the PCL chain axis is perpendicular to the stretching direction in PCL/PVC blends melt crystallized under strain [8]. This kind of orientation is different from the conventional WAXD patterns observed experimentally for

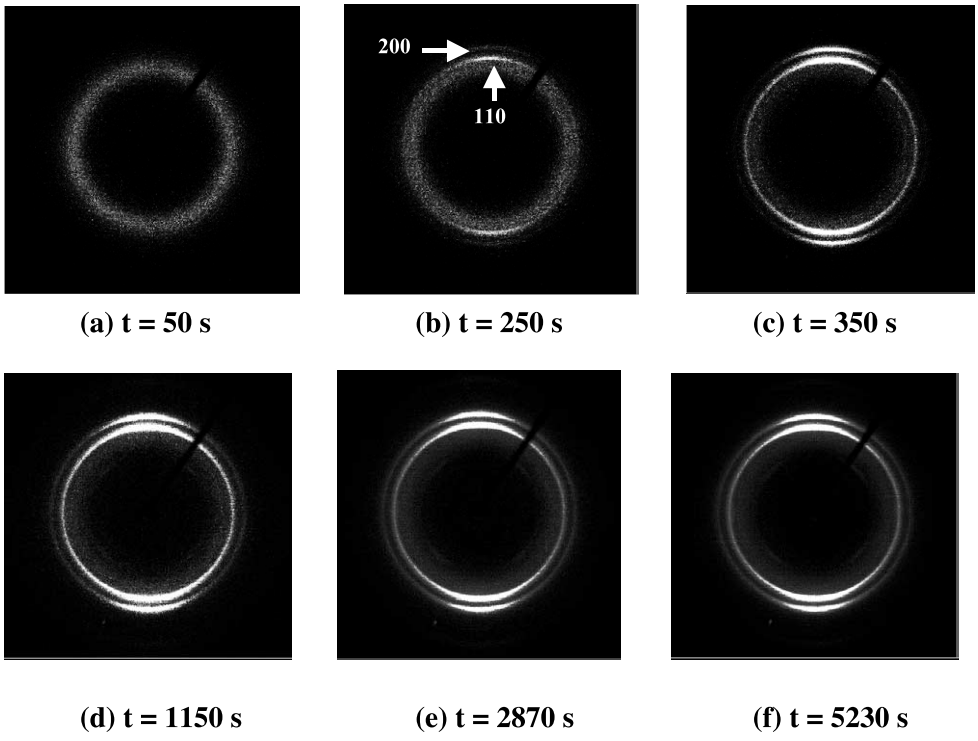

Fig. 2. Typical WAXD patterns recorded at various times after a PCL/PVC-80/20 blend film was stretched to $\lambda = 3.6$ and cooled to room temperature under strain. (a) $t = 50$ s, (b) $t = 250$ s, (c) $t = 350$ s, (d) $t = 1150$ s, (e) $t = 2870$ s and (f) $t = 5230$ s.

uniaxially stretched polymer samples in which the crystal *c*-axis is more or less oriented to the stretching direction.

However, this raises the question about how the (110) and (200) reflections and the crystal *c*-axis are distributed in the three-dimensional space. It is difficult to visualize how both (110) and (200) reflections, which are at an angle of 56.4° to each other, orient to the same direction of stretching and, at the same time, how the crystal *c*-axis is kept perpendicular to the stretching direction. In fact, this kind of orientation can be attributed to what Kakudo and Kasai called ring-fibre orientation [15]. This is a case when the crystal *c*-axis is perpendicular to the stretching direction but the crystal *a*- and

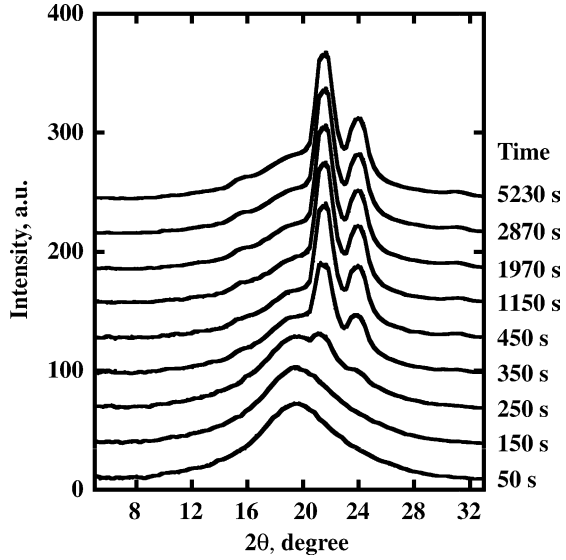

Fig. 3. Azimuthally averaged WAXD intensity profiles at various times after a PCL/PVC-80/20 blend film was stretched to $\lambda = 3.6$ and cooled to room temperature under strain.

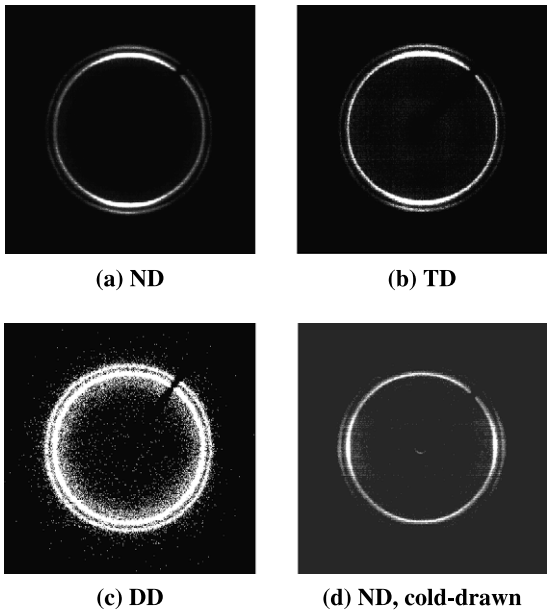

Fig. 4. Typical WAXD patterns along (a) ND, (b) TD and (c) DD-directions for a PCL/PVC-80/20 blend sample crystallized from a pre-oriented melt ($\lambda = 3.6$). The WAXD pattern along the ND-direction of a PCL/PVC blend sample crystallized from quiescent melt and, then, stretched at room temperature (~22 °C) to a similar draw ratio is also shown for comparison (d).

b-axes are randomly oriented. A similar unusual orientation has been observed in a recent publication about the effect of magnetic field on the crystal orientation of polystyrene, in which a detailed representation of the diffraction pattern from a reciprocal lattice has been proposed [16].

A real space representation of the ring-fibre orientation is shown in Fig. 5(a). On the one hand, the crystal *c*-axis keeps perpendicular to the stretching direction (the vertical direction); on the other hand, both the crystal *a*- and *b*-axes randomly distribute in a plane perpendicular to the crystal *c*-axis. As a result, the intensities of (*hk*0) reflections are proportional to 1/sin χ, where χ is the azimuthal angle, and peaks with a finite width are observed [Fig. 5(b)] in the meridional direction [16]. This kind of orientation is very similar to the case of row orientation, a special type of uniaxial orientation frequently observed when polyethylene crystallizes from an oriented melt [17–20]. The difference is, in the case of row orientation, it is the crystal *b*-axis, instead of the crystal *c*-axis, keeps perpendicular to the stretching direction, while the crystal *a*- and *c*-axes evenly distribute in a plane perpendicular to the crystal *b*-axis.

For these (*hkl*) reflections with $l \neq 0$, i.e. at acute angles to the crystal *c*-axis, the ring-fibre orientation gives rise to two arcs or spots intersecting the equator and extending systematically above and below the equator [Fig. 5(c)] [15,16]. Unfortunately, in our experiments, the (*hkl*) reflections with $l \neq 0$ are either too weak, or seriously overlap with other reflections. Nevertheless, the weak (102) reflection ($2\theta = 16°$) at $\chi \sim 40°$ can be interpreted as the consequence of ring-fibre orientation [Fig. 2(d)–(f), and more clearly in Fig. 6 below], because the (102) reflection is expected at an angle of 49.1° to the crystal *c*-axis.

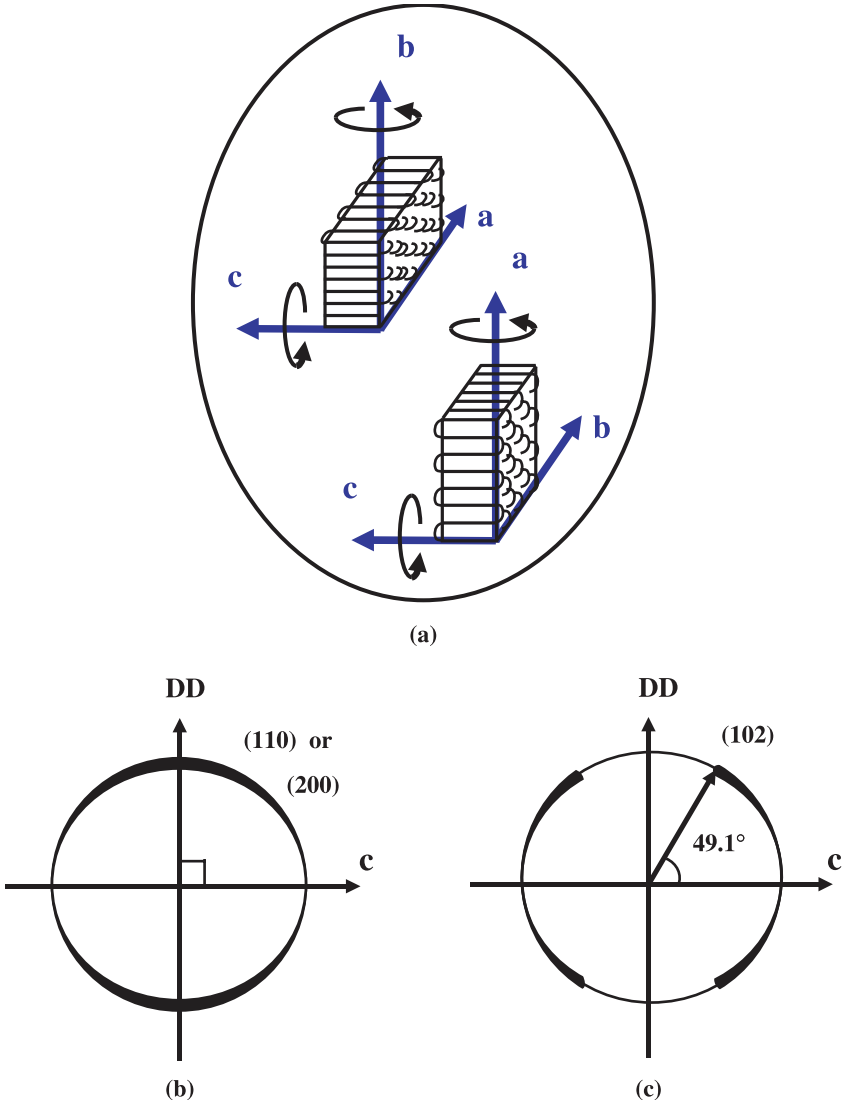

Fig. 5. Schematic diagrams of crystal orientation in a ring-fibre orientation: (a) a real space representation of the ring-fibre orientation; (b) diffraction pattern from (110) and (200) reflections perpendicular to the crystal *c*-axis; (c) diffraction pattern from the (120) reflection which is at an angle of 49.1° to the crystal *c*-axis.

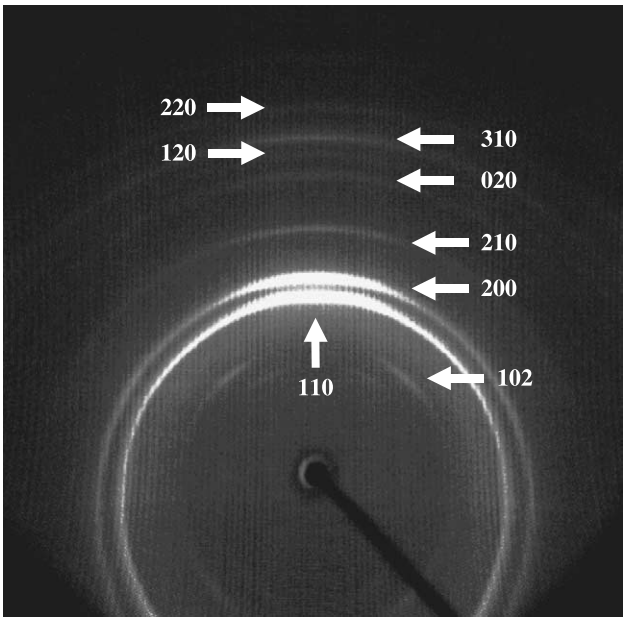

Fig. 6. WAXD pattern of a PCL/PVC-80/20 blend for which the detector was off-set in order to show the reflections at wider diffraction angles in the meridional direction.

Fig. 6 shows the WAXD pattern of a PCL/PVC-80/20 blends melt crystallized under strain in which the detector was off-set in order to show the crystal reflections at wider diffraction angles ($2\theta = \sim 5$–60°) in the meridional direction. In addition to the strong (110) and (200) reflections, some crystal reflections are clearly seen at $2\theta = 29.9$, 36.1, 38.1, 40.4, and 43.7° in the meridional direction. These weak reflections have been indexed (210), (020), (120), (310) and (220), as indicated in Fig. 6. All these *hk*0 reflections are perpendicular to the crystal *c*-axis, indicating a perpendicular *c*-axis to the stretching direction. These observations, together with the above-mentioned (102) reflection at $\chi \sim 40^\circ$, strongly support the presence of ring-fibre orientation.

3.3. Effect of PVC content on the crystal orientation of PCL/PVC blends

Fig. 7 shows typical WAXD patterns for PCL/PVC blends of 80/20, 70/30 and 60/40 compositions, respectively, at a draw ratio of 4.0. The WAXD patterns for PCL/PVC blends with higher PVC contents are very similar to those shown in Figs. 2 and 4. The occurrence of the two (110) and (200) reflections center at the meridian gives a strong indication of the perpendicular orientation of the crystal *c*-axis to the stretching direction. Additional peaks emerge at $\chi \sim 55^\circ$ on the first quadrant of the (110) reflection ring, and at $\chi \sim 65^\circ$ on the first quadrant of the (200) reflection ring. These new peaks, whose intensity increases with the increase of PVC content in the PCL/PVC blends, can be seen more clearly in the azimuthal profiles shown in Fig. 8. From the PCL crystal structure, the (110) reflection is expected at an angle of 56.4° away from the crystal *a*-axis. The newly emerging peak at $\chi \sim 55^\circ$ on the (110) reflection ring can then be interpreted as a consequence of the crystal *a*-axis orientation, i.e. the (200) reflection orients to the stretching direction.

The strong reflection ring at $2\theta = 23.7^\circ$ is generally attributed to the (200) reflection of PCL [10]. A close examination of the PCL crystal structure, however, reveals that this reflection ring is actually made of the overlapped (200), (112), (013) and (104) reflections, with Bragg angles at 23.7, 23.8, 23.6, and 23.7°, respectively, the (200) reflection being much stronger than the others [9]. Apparently, these reflections are too close to be separated, and their intensities are non-negligible as compared with that of the (200) reflection, especially in an oriented sample, in which the overlapped reflections could be well separated. For example, if the crystal *a*-axis is oriented in the stretching direction, both (112) and (104) reflections would be located at $\chi \sim 60^\circ$, and their added intensity could be as high as 30% of the intensity of the (200) reflection from structure factor calculation [9]. Therefore, we attribute the new peak around $\chi \sim 65^\circ$ on the reflection ring at $2\theta = 23.7^\circ$ to the overlapped intensity of (112) and (104) reflections. In other words, the observed new peak at $\chi \sim 65^\circ$ on the (200) reflection ring is in fact accords with the emergence of the peak at $\chi \sim 55^\circ$ on the (110) reflection ring, which is due to the orientation of the crystal *a*-axis to the stretching direction. The WAXD patterns observed are actually the superposition of the crystal *a*-axis orientation and the ring-fibre orientation, but the later

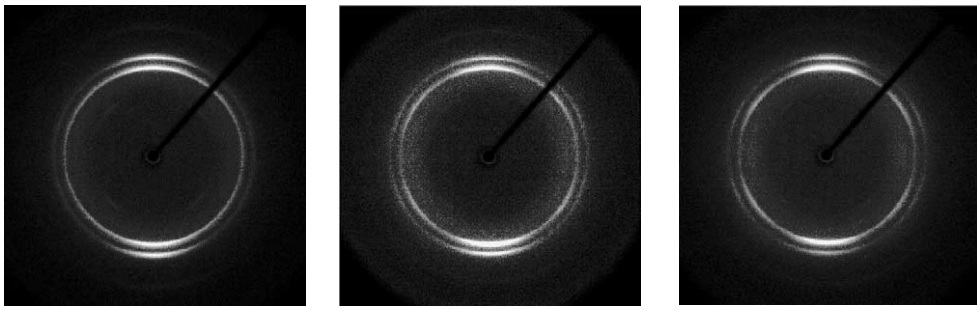

(a) 80/20 **(b) 70/30** **(c) 60/40**

Fig. 7. WAXD patterns of PCL/PVC blends with PVC contents of (a) 20, (b) 30 and (c) 40 wt%; the draw ratios are $\lambda \sim 4.0$.

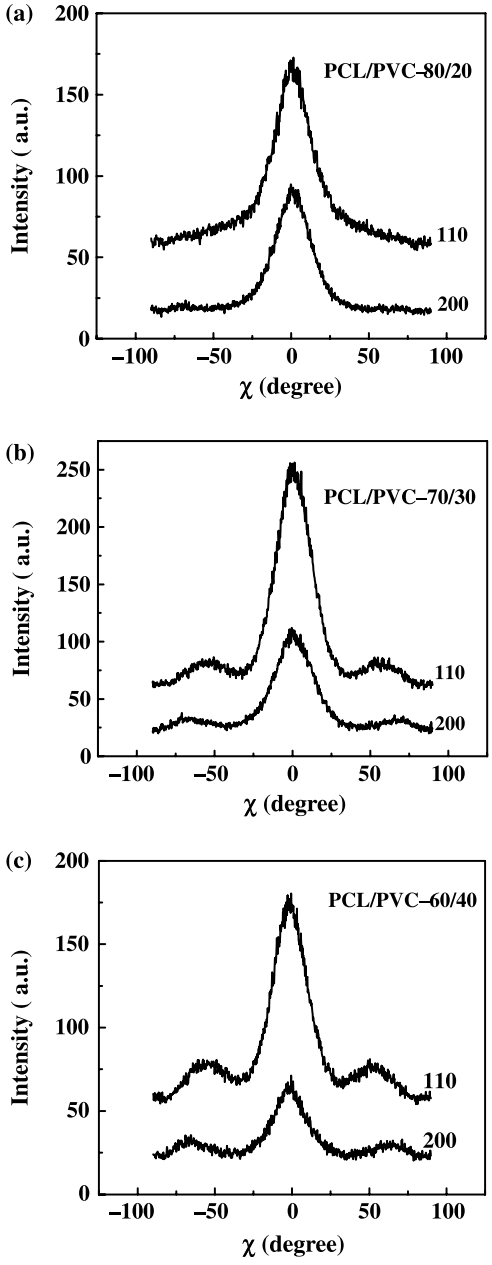

Fig. 8. Azimuthal profiles of WAXD patterns of Fig. 7.

dominates the patterns. A real space representation of the *a*-axis orientation are showed in Fig. 9, in which the crystal *a*-axis is parallel to the stretching direction, while the crystal *b*- and *c*-axes randomly distribute in a plane perpendicular to the stretching direction.

3.4. Orientation as a function of draw ratio

Fig. 10 shows the WAXD patterns of PCL/PVC-70/30 blends melt crystallized under strain at different draw ratios. The corresponding azimuthal profiles for both the (110) and (200) reflections are displayed in Fig. 11. All the WAXD patterns show strong (110) and (200) reflections around the meridional direction, indicating the perpendicular orientation of the crystal *c*-axis for PCL/PVC-70/30 blends with various draw ratios. With the increase of draw ratio, additional peaks emerge at $\chi \sim 55$ and $\sim 65^\circ$ on the first quadrants of the (110) and (200) reflection rings, respectively. At the same time, the (110) and (200) reflections centered in the meridional direction become slightly sharper, indicating an increasing degree of crystal *c*-axis orientation in the direction perpendicular to the stretching direction. Interestingly, the peak areas of the (110) reflection at $\chi \sim 55^\circ$ and the (200) reflection at $\chi \sim 65^\circ$ change little with an increase of draw ratio after $\lambda = 2.7$. Actually, the ring-fibre orientation dominates the WAXD patterns even at high draw ratios and high PVC contents. These observations demonstrate that the increase of draw ratio is qualitatively equivalent to an increase of PVC content in the PCL/PVC blends. Both of them facilitate the formation of the *a*-axis orientation of PCL crystals in blends.

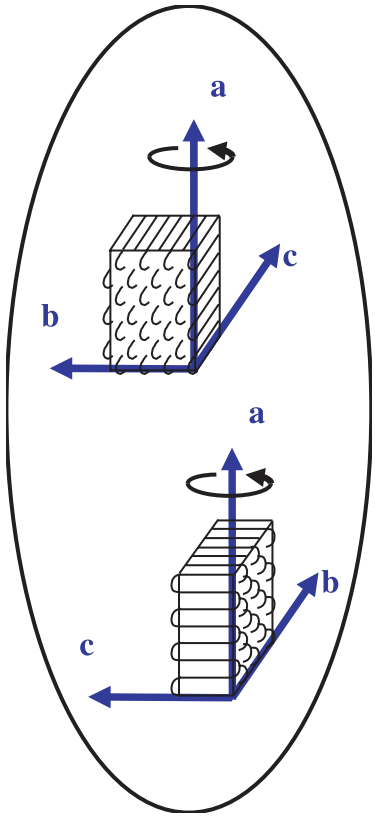

Fig. 9. A real space representation of the *a*-axis orientation, in which the crystal *a*-axis is parallel to the stretching direction, while the crystal *b*- and *c*-axes randomly distribute in a plane perpendicular to the stretching direction.

For a single parameter characterization of the influence of draw ratio on the orientation of PCL crystals, Herman's orientation functions for individual crystal axes, $\langle P_2 \rangle_a$, $\langle P_2 \rangle_b$ and $\langle P_2 \rangle_c$, have been calculated, and are shown in Fig. 12. $\langle P_2 \rangle_c$ is close to -0.5 for the PCL/PVC-70/30 blend above a draw ratio of ~ 3.0, which is the theoretical limit for a perfect perpendicular orientation. The positive $\langle P_2 \rangle_a$ is a consequence of the presence of the *a*-axis orientation, as

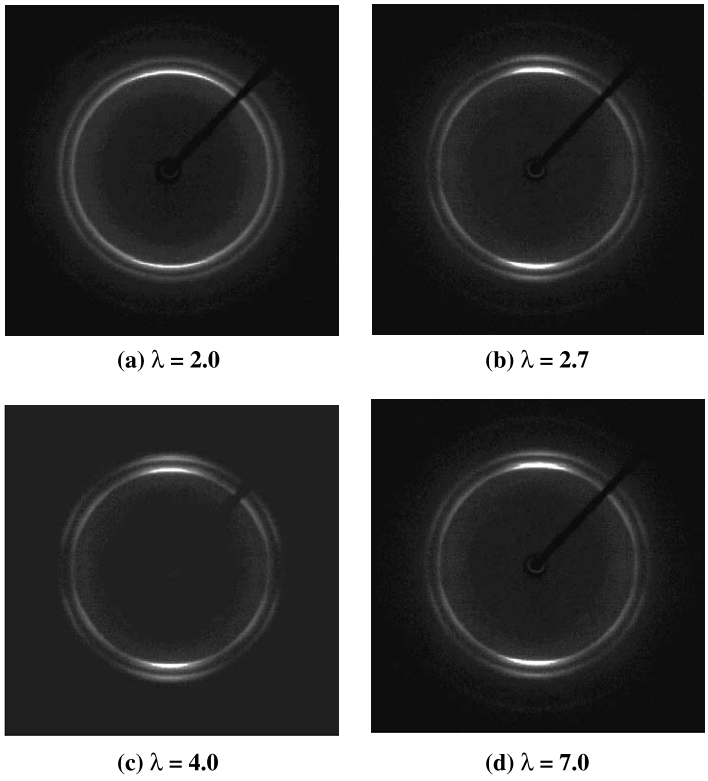

Fig. 10. WAXD patterns for PCL/PVC-70/30 blends melt crystallized at draw ratios of (a) 2.0, (b) 2.7, (c) 4.0, and (d) 7.0.

was observed in polyethylene crystallization under strain of low elongation [21]. The nearly zero or small negative $\langle P_2 \rangle_b$ indicates that the crystal *b*-axis slightly deviates from the random distribution in a plane perpendicular to the crystal *c*-axis (i.e. the case of the ring-fibre orientation). This is in agreement with the low degree of crystal *a*-axis orientation with respect to the stretching direction.

4. Discussion

Two kinds of crystal orientations, i.e. the ring-fibre orientation and the *a*-axis orientation, are observed in PCL/PVC blends crystallized under strain. Both of them are characterized by a perpendicular orientation of the crystal *c*-axis with respect to the stretching direction. In all cases, the ring-fibre orientation dominates the WAXD patterns, but it does more at low draw ratios and low PVC contents. With the increase of draw ratio or PVC content, the crystal *a*-axis changes its orientation and begins to orient preferentially to the stretching direction. Therefore, the PCL crystal orientation is a consequence of the combined effects of stretching and the presence of PVC in the blends.

Oriented crystallization in polymers has been widely described by the row orientation model of Keller and Machin [17–20]. According to this model, the 'flow lines' induced by deformation act as nucleation center for lamellae growth as they do in a spherulite, i.e. with the crystal *b*-axis parallel to the growth axis. At low stress, lamellae grow with an uniform twist, which is equivalent to the random distribution of both the crystal *a*- and *c*- axes in a plane perpendicular to the crystal *b*-axis, and leads to the parallel orientation of both *a*- and *c*-axes to the stress direction. At high stress, the lamellae grow in regular flat ribbons without twisting, which results in the crystal *c*-axis being oriented preferentially along the stress direction. Intermediate stresses lead to an incomplete twisting of the lamellae ribbons. For example, the lamellae growth in a non-uniform twist with 'large flat-on-view portions' according to Keller and Machin's jargon, can lead to crystal orientation with the crystal *a*-axis parallel to the stress direction. Although the *a*-axis orientation in PCL/PVC blends crystallized under strain can be explained by the row orientation model with lamellae having 'large flat-on-view portions', the majority ring-fibre orientation that has been observed cannot be explained by this model.

It is well-known that the two polymer components of amorphous miscible polymer blends following cold drawing can orient differently despite their miscibility. This behaviour has been interpreted in terms of the difference between the flexibility of the two chains involved and the subsequent differences in relaxation of the oriented chains. For PCL/PVC blends, it has been found that the PCL chains relax much faster than the PVC chains [8]. Highly aligned lamellae with crystalline chains oriented perpendicular to the stretching direction were observed in miscible PCL/PVC blends with the PVC highly oriented and the PCL component almost relaxed to an unoriented state [8]. It is

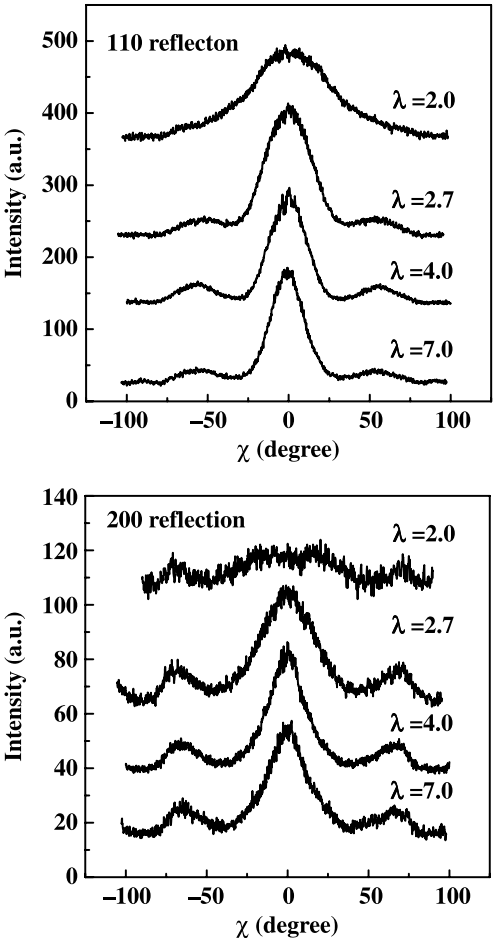

Fig. 11. Azimuthal profiles of (110) and (200) reflections for PCL/PVC-70/30 blends melt crystallized at draw ratios of 2.0, 2.7, 4.0 and 7.0.

unlikely that the 'follow-lines', which act as nuclei according to Keller and Machin's row orientation model, would form in PCL/PVC blends with almost unoriented PCL melt. If we assume the presence of row nucleation in such a low oriented PCL melt, the lamellae are expected to grow with an uniform twisting, leading to the row

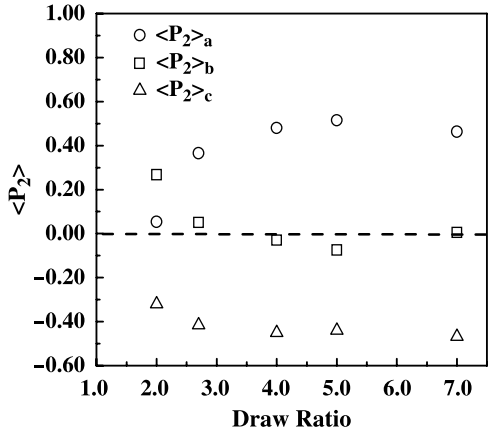

Fig. 12. Orientation functions of individual crystal axes as a function of draw ratio for PCL/PVC-70/30 blends.

orientation, in which the crystal *b*-axis is perpendicular to the stretching direction. This is not the case since the WAXD analysis of PCL/PVC blends crystallized under strain indicates that the crystal *b*-axis is oriented parallel to the stretching direction in the ring-fibre orientation. Similarly, in IR dichroism analysis [20], the row orientation gives a net orientation of the crystal *c*-axis parallel to the stretching direction, whereas in the ring-fibre orientation, IR dichroism revealed the perpendicular orientation of the crystal *c*-axis to the stretching direction [8].

Crystallization with the crystal *c*-axis perpendicular to the deformation direction has also been found in the fibre spinning of polypropylene fibre [22–25]. The occurrence of perpendicular crystal *c*-axis orientation has been attributed to homoepitaxy crystal growth on the lateral ac-faces of the α-crystalline polypropylene, which resulted in lamellar branching of crystals in the daughter lamellae with their *a**-axis in the flow direction. A bimodal crystalline orientation is usually clearly distinguished from WAXD patterns since the (110) reflection of the α-crystalline polypropylene at $2\theta = 14.4°$ is made of two contributions: an equatorial component and a component close to the meridian. Apparently, this is not the case in PCL/PVC blends, as the two (110) reflection populations (at $\chi \sim 0$ and $\sim 55°$) in the WAXD patterns indicate the same phenomenon of perpendicular orientation of the crystal *c*-axis to the stretching direction; however, one of them indicates the presence of a ring-fibre orientation, while the second one is related to the *a*-axis orientation.

A perpendicular orientation of chain axis to the deformation direction has also been observed in block copolymers, in which one or both components are crystallisable [26–29]. This kind of orientation was believed to be thermodynamically stable and has been employed to formulate different theoretical approaches [30,31]. In a recent systematic study on the orientation of poly(ethylene oxide) crystals in diblock copolymer of poly(ethylene oxide-*b*-polystyrene) as a function of crystallization temperature, the perpendicular orientation was believed to be determined by the combined effect of nucleus density and nano-confinement [32]. In the case of miscible A/B polymer blends, the possibility of nano-scale confinement has been recently explored, and the confined crystallization of blend component A was shown to occur in between the B lamellae [33]. Unusual crystal orientation with the fastest growth axis, i.e. the crystal *b*-axis, oriented parallel to the stretching direction, was also observed in the miscible blend of poly(1,4-butylene succinate) and poly(vinylidene fluoride) [33]. Therefore, nano-confined crystallization, if present in PCL/PVC blends, would result in preferential orientation of the crystal *b*-axis, or the (110) crystal plane, instead of the crystal *a*-axis to the deformation direction as these directions are usually the fastest growth crystal plane. This is contrary to the observations made in this study.

In a previous paper, following IR results, we proposed to use Judge and Stein's intramolecularly nucleation model to

explain the unusual orientation in PCL/PVC blends crystallized under strain [8]. According to this model, nuclei can be formed by chain retracting and then folding along the chain direction at low draw ratio [21]. A direct consequence of the folding along the chain direction is the orientation of the crystal *a*-axis to the stretching direction, as the crystal *a*-axis is defined being parallel to the chain folding direction (Fig. 9). Although this mechanism agrees well with the IR results and the current WAXD observation about the *a*-axis orientation, it cannot explain the ring-fibre orientation. Judge and Stein' model was proposed to explain the perpendicular chain orientation in a cross-linked polyethylene crystallized at low draw ratios. It did not consider the role of non-crystallisable PVC component on the PCL crystal orientation. Further studies are in progress, which focus on the role of PVC to develop a new model that can explain not only the *a*-axis orientation but also the ring-fibre orientation in the PCL/PVC blends crystallized under strain.

5. Conclusion

The wide angle X-ray diffraction analysis confirms that the polymer chain direction of PCL crystals in miscible PCL/PVC blends crystallized under strain is preferentially oriented perpendicular to the stretching direction. However, the orientation function is much more complex than it was inferred previously from IR dichroism. Two kinds of crystal orientations, i.e. the ring-fibre orientation and the *a*-axis orientation, are observed. Both of them are characterized by perpendicular orientation of the crystal *c*-axis to the stretching direction, with the former dominating the WAXD patterns. The ring-fibre orientation is preferentially formed at low draw ratios and low PVC contents, in which both the crystal *a*- and *b*-axes are randomly distributed in a plane perpendicular to the crystal *c*-axis, with the crystal *c*-axis itself randomly distributed in a plane perpendicular to the stretching direction. With the increase of draw ratio or PVC content, the crystal *a*-axis is found to orient preferentially to the stretching direction. A quantitative description of PCL crystal orientation has been given in term of the orientation functions ($\langle P_2 \rangle$) of individual crystal axes. The PCL crystal orientation in PCL/PVC blends melt crystallized under strain differs from that found in cold-drawn semi-crystalline polymers, or that found in the crystallization from conventional pre-oriented polymer melts.

Acknowledgements

The financial support of NSERC (Canada) and FCAR (Québec) is gratefully acknowledged.

References

[1] Keller A, Kolnar HW. Mater Sci Technol 1997;18:189.
[2] Lee O, Kamal MR. Polym Eng Sci 1999;39:236.
[3] Schultz JM. The development of crystalline order in thermoplastic polymers. New York: Oxford University Press; 2001.
[4] Eder G, Janeschitz-Kriegl H. Mater Sci Technol 1997;18:268.
[5] Liedauer S, Eder G, Janeschitz-Kriegl H. Int Polym Process 1995;10:243.
[6] Kumaraswamy G, Issaian AM, Kornfield JA. Macromolecules 1999;32:7537.
[7] Ania F, Bayer RK, Tschmel A, Michler HG, Naumann I, Baltá-Calleja FJ. J Mater Sci 1996;31:4199.
[8] Zhao Y, Keroack D, Prud'homme RE. Macromolecules 1999;32:1218.
[9] Bittiger H, Marchessault RH, Niegisch WD. Acta Cryst 1970;B26:1923.
[10] Ong CJ, Price FP. J Polym Sci, Polym Symp 1978;63:45.
[11] Polanyi M. Z Phys 1921;7:149.
[12] Ward IM. Developments in oriented polymers-1. London: Applied Science Publishers; 1982.
[13] Deas HD. Acta Cryst 1952;5:542.
[14] Lovell R, Mitchell GR. Acta Cryst 1981;A37:135.
[15] Kakudo M, Kasai N. X-ray diffraction by polymer. London: Elsevier; 1972.
[16] Ebert F, Thurn-Albrecht T. Macromolecules 2003;36:8685.
[17] Baltá-Calleja FJ, Vonk CG. X-ray scattering of synthetic polymers. Amsterdam: Elsevier; 1989 [chapter 6].
[18] Dees JR, Spruiell JE. J Appl Polym Sci 1974;18:1053.
[19] Keller A. J Polym Sci 1955;15:31.
[20] Keller A, Machin MJ. J Macromol Sci (Phys) 1967;B1:41.
[21] Judge JT, Stein RS. J Appl Phys 1961;32:2357.
[22] Clark ES, Spruiell JE. Polym Eng Sci 1976;16:176.
[23] Sakthivel A, Abhiraman AS. J Appl Polym Sci 1984;29:4257.
[24] Fujiyama M, Wakino T. J Appl Polym Sci 1991;42:9.
[25] Goschel U, Swartjes FHM, Peters GWM, Meijer HEH. Polymer 2000;41:1541.
[26] Lotz B, Kovacs AJ, Bassett GA, Keller A. Kolloid-Z Z Polym 1966;209:115.
[27] Kovacs AJ, Lotz B, Keller A. J Macromol Sci Phys 1969;B3(3):385.
[28] Hirata E, Ijitsu T, Hashimoto T, Kawai H. Polymer 1975;16:249.
[29] Yang YW, Tanodekaew S, Mai SM, Booth C, Ryan AJ, Bras W, et al. Macromolecules 1995;28:6029.
[30] DiMarzio EA, Guttman CM, Hoffman JD. Macromolecules 1980;13:1194.
[31] Whitmore MD, Noolandi J. Macromolecules 1988;21:1482.
[32] Zhu L, Cheng SZD, Calhoun BH, Ge Q, Quirk RP, Thomas EL, et al. J Am Chem Soc 2000;122:5957.
[33] He Y, Zhu B, Kai W, Inoue Y. Macromolecules 2004;37:3337.